

A Highly Flexible and Scalable S-band SwarmSAR from Very Simple Nodes

Iannini, Lorenzo; Lopez-Dekker, Paco; Hoogeboom, Peter

DOI

[10.1109/RadarConf2043947.2020.9266527](https://doi.org/10.1109/RadarConf2043947.2020.9266527)

Publication date

2020

Document Version

Final published version

Published in

2020 IEEE Radar Conference, RadarConf 2020

Citation (APA)

Iannini, L., Lopez-Dekker, P., & Hoogeboom, P. (2020). A Highly Flexible and Scalable S-band SwarmSAR from Very Simple Nodes. In *2020 IEEE Radar Conference, RadarConf 2020* Article 9266527 (IEEE National Radar Conference - Proceedings; Vol. 2020-September). IEEE.
<https://doi.org/10.1109/RadarConf2043947.2020.9266527>

Important note

To cite this publication, please use the final published version (if applicable).
Please check the document version above.

Copyright

Other than for strictly personal use, it is not permitted to download, forward or distribute the text or part of it, without the consent of the author(s) and/or copyright holder(s), unless the work is under an open content license such as Creative Commons.

Takedown policy

Please contact us and provide details if you believe this document breaches copyrights.
We will remove access to the work immediately and investigate your claim.

A Highly Flexible and Scalable S-band SwarmSAR from Very Simple Nodes

Lorenzo Iannini

Department of Geoscience and Remote Sensing

Delft University of Technology

Delft, The Netherlands

l.iannini@tudelft.nl

Paco Lopez-Dekker

Department of Geoscience and Remote Sensing

Delft University of Technology

Delft, The Netherlands

f.lopezdekker@tudelft.nl

Peter Hooeboom

Department of Geoscience and Remote Sensing

Delft University of Technology

Delft, The Netherlands

p.hooeboom@tudelft.nl

Abstract—The paper introduces the principles and the technical elements supporting the so-called SwarmSAR concept, consisting in a close formation of simple nodes cooperating in a MIMO-like frame to boost their imaging flexibility and performance. The philosophy of the swarm consists in employing extremely basic but self-sufficient nodes, each one guaranteeing sufficient image quality even when used individually. The costs are hence diverted from the node to the formation launching and maintenance aspects. We promote in this paper the use of S-Band as a convenient frequency both for the single node and for the formation requirements and resourceful for applications. An outline of the envisioned cooperative illumination modes, including high resolution imaging and the interferometric modes, and a preliminary discussion on their expected performance and challenges is provided.

Keywords—SAR, small satellites, swarm, multistatic, S-Band, mini-Sat.

I. INTRODUCTION

In the last few years, several SAR (Synthetic Aperture Radar) satellite imagers have been investigated and implemented in a wide range of size and complexity scales, with < 100 kg mini satellites [1, 2] on one side, small-sized satellites, such as NovaSAR-S [5], in the middle, and 1000+ kg satellites with advanced beam forming capabilities [3, 4] on the other side. So far, the rationale of mini satellite missions has not been to outperform the big-sized satellites in terms of global coverage or image quality, but rather to offer competitive imaging at affordable costs and fast temporal revisit in a limited number of spots. Such missions rely therefore on large constellations.

The SwarmSAR concept hereafter presented, when compared to a single satellite SAR, takes a significantly different turn in terms of philosophy. The SwarmSAR concept aims at pushing even further the miniaturization and the simplicity of the single nodes, building up a variety of flexible and higher quality products from the multi-static nodes cooperation. The key feature of the mission consists indeed in the multi-static radar capabilities. Multi-channel systems represent one of the most appealing options for future SAR satellite missions owing to their flexibility, cost-effectiveness and enhanced imaging capabilities. A few multiple-platform concepts have been so far promoted, either operating in SIMO mode, with one transmitter and multiple receivers [6], or implementing a MIMO scheme, with transmitting and receiving capabilities embedded in all units [7, 16]. The added values of such operating schemes appear obvious. With respect to a single antenna instrument, a SIMO system would potentially increase the performance/capabilities by a factor

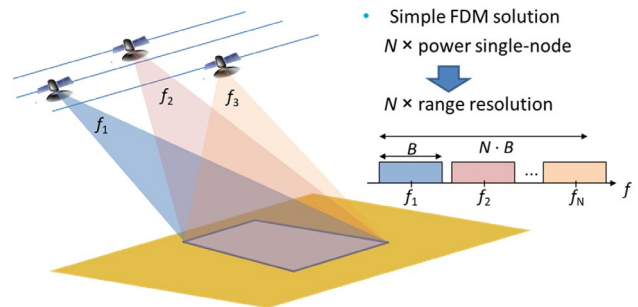


Fig. 1. Sketched representation of a MIMO system where FDM is employed for transmission. The Rx bandwidth of the instruments shall be wide enough to accommodate all the spectral components (approximately N times the bandwidth B of a single channel).

N , where N is the number of antennas, whereas a MIMO scheme would introduce a N^2 boost (when all N antennas work in both Tx and Rx), due to an increase in bandwidth (and power). Besides, the MIMO scheme enhances the robustness of the system to eventual failures in one of the transmitting units.

In a SwarmSAR the N satellites are expected to fly in a string-of-pearls formation, with a short along-track separation (a fraction of the critical bandwidth to coherently combine the channels) and illuminate a common footprint, i.e. all the antennas will be pointed to the same area on the ground. The illumination capabilities of each node shall remain extremely basic (no beam steering, low power), but still sufficient to perform decent stripmap imaging when operated individually. Each node shall carry as main payload an S-Band microwave instrument with both transmit and receive functionalities. The simultaneous node transmission is then carried out through a Frequency Division Multiplexing (FDM) strategy, as sketched in Fig. 1. The formation would enable the following cooperative modes/products: 1) a high resolution imaging mode, 2) a XTI/ATI interferometric mode.

The document is structured as follows. Section II will elaborate on the single node design choices and its self-standing performance. Section III and IV will focus on the potential of the SwarmSAR in high-resolution (HR) imaging and cross-track interferometry (XTI) respectively. The paper is then concluded by a short discussion on the challenges awaiting in section V.

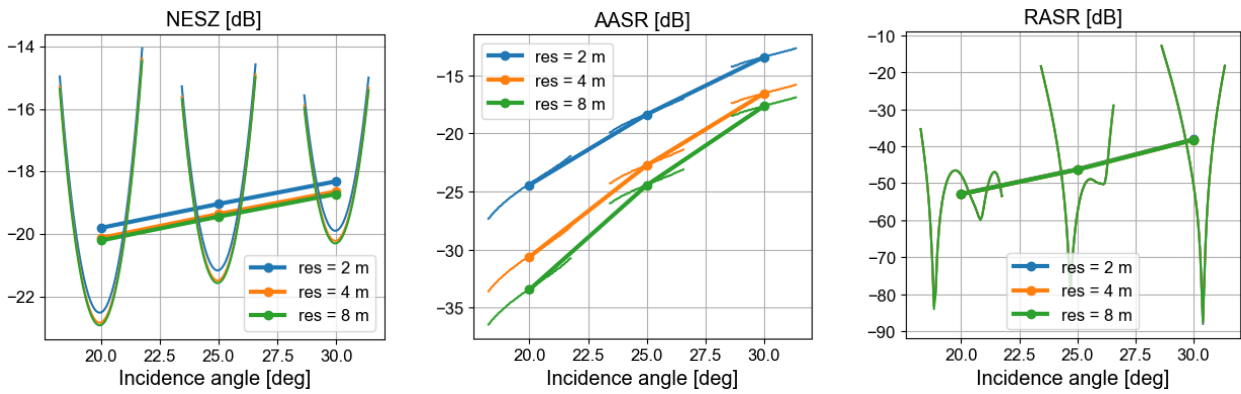


Fig. 2. Single node performance as a function of the incidence angle (with system parameters in table 1). The PRF and the swath width for the tested angles, 20°, 25° and 30°, are reported in Table 2.

II. NODE DESIGN

The SwarmSAR philosophy leverages on three fundamental principles:

- “The nodes are extremely simple in terms of illumination capabilities (stripmap)”
- “The nodes are all equal”
- “The nodes are self-sufficient, i.e. they are able to form an image with decent quality (NESZ (Noise Equivalent Sigma Zero) and DTAR (Distributed Target Ambiguity Ratio) < -15 dB) when operated individually”

The first statement implies that no complex beam steering or digital beam-forming capabilities will be implemented. Antenna agility usually comes at a cost in terms of weight and size. The size is in particular the most influential parameter on the system performance. In order to maintain the design as low-swap (low size, weight and power) as possible, we shall aim for an antenna surface/weight ratio of 1-1.5 m²/kg. Such a value is extremely challenging for antennas of relatively large sizes (>3 m²) in mini satellites, where several mechanical problems can be encountered [11]. The baseline scenario for our concept is a reflector-based antenna with a circular dish, illuminated by a single feed. The agility in beam elevation (in order to increase access rate) shall be then obtained by mechanical platform maneuvering.

The second principle advocates for a symmetric node formation. Evident asymmetries, such as in the MirrorSAR concept [6], shall be then avoided. This principle applies to the whole platform, not only to the SAR payload. In other words, all the nodes shall be interchangeable with no loss of efficiency or performance. This would also allow to reduce the complexities in manufacturing, launching and maintenance processes and hence to scale up (cost-)efficiently the system.

The third condition affects the size, power and weight of the node. As insightfully elaborated in [10], the instrument design consists in a trade-off design exercise. This led in our case to the baseline node specifications reported in Table 1. A noteworthy outcome is the choice of the frequency: S-Band is indeed deemed the most convenient band from the trade-off between antenna simplicity (circular dish), coverage and power. Higher frequencies would require elongated antenna shapes. Further performance analysis conveys that a Ø 2 m reflector antenna is a minimum requirement for AASR

Table 1. S-Band node specifications

Parameter	Value
Frequency	3.2 GHz
Average Tx power	20W
Pulse Length	20 µs
Antenna	Reflector Ø 2 m Directivity: 36 dB Beam width: 3.2°
Bandwidth	20 MHz
Orbit height	514 km

performance in S-Band. This is confirmed by the small (but still appreciable, 1 dB at 30°) performance difference in the second panel of Fig. 2 by reducing the azimuth resolution (and thus the processed azimuth bandwidth) from 4 m to 8 m. The access angle is currently limited to 30°. Above 25°, the azimuth bandwidth shall be constrained to 4 m resolution to maintain acceptable AASR, unless the scene backscatter dynamics allow otherwise. Notice, from the values in Table 2, that the swath width on the ground decreases rather than increase with the incidence angle. Due to the critical PRF sampling, the range ambiguities impair significantly a portion of the swath (that portion was not included in the calculation). Fig. 2 shows the narrow angular width of RASR at 30°. The NESZ is evaluated through the well-known relationship [14]

$$NESZ = \frac{2(4\pi)^3 \cdot R^4 \cdot k_B \cdot T_{sys} \cdot B \cdot \sin \eta}{c_0 \lambda^2 \cdot \epsilon \cdot P_{av} \cdot G_0^2 \cdot \delta_{az} \cdot G_{pat}} \quad (1)$$

where R is the slant range, k_B is the Boltzmann’s constant, T_{sys} is the system temperature (set to 560 K), B is the bandwidth, η is the local incidence angle, c_0 is the speed of light, λ is the wavelength, ϵ is the system efficiency (set to 0.5), P_{av} is the average power, G_0 is the antenna gain, δ_{az} stands for the azimuth resolution and G_{pat} , defined as $G_{pat} = |C_{2way,el}(\theta) \sum_{i=1}^{N_a} C_{2way,az}(\phi)|^2 / N_{az}$, accounts for the normalized antenna patterns, in azimuth and elevation, over the N_{az} samples within the integrated Doppler bandwidth. The slight performance differences reported in Fig. 2 for different azimuth resolutions are hence imputable to the decrease in SNR at higher Doppler frequencies. As for the

Table 2. Performance for single-node and HR SwarmSAR imaging averaged within the considered swath. The expected performance is computed for the system parameters specified in Table 1. The DTAR entries shall be considered as average performance in the worst case scenario, i.e. no PRF optimization is applied to the system. The resolution is expressed as ground range by azimuth.

Mode	# Sat	Inc. Ang. [deg]	Swath Width [km]	Res _{rg, az} [m]	PRF [Hz]	NESZ [dB]	DTAR [dB]
Single	1	20	32	22, 2	8670	-20	-24
		25	31	18, 2	7850	-19	-18
		30	29	15, 4	7030	-18.5	-16
HR (MIMO)	3	20	32	7, 1	8670	-22.5	-26
		25	35	6, 1	7060	-21	-24
		30	38	5, 1	5750	-20	-20
HR (MIMO)	6	25	35	3, 1	7060	-24	-26
		30	38	2.5, 1	5750	-23	-26
		35	42	2.2, 1	4740	-21.5	-24
		40	48	2, 1	4010	-20	-20

DTAR performance metrics, the NESZ becomes poor for angles larger than 30°, being limited by the ground resolution.

III. SWARMSAR HR IMAGING

The SwarmSAR imaging leverages on the concept of Displaced Phase Center (DPC) processing [8]. In a MIMO acquisition scenario, for each of the N transmitters, a set of N pulse sequences is available, one for each receiver, with azimuth phase centers spaced by approximately half of the along-track (AT) baselines, as shown in Fig. 3. Within an FDM transmission scheme, a MIMO system shall be regarded as N SIMO systems. For each SIMO, ideally, we would like these phase centers to satisfy a perfect pulse interleave scenario and thus a regular azimuth sampling. In the simple case of $N = 2$ satellites, any $(k + 0.5)$ PRI offset between the antenna phase centers would lead to a uniformly sampled signal with double PRF, and hence to an optimal ambiguity rejection. With $N > 2$ satellites a PRF satisfying the uniform sampling condition, given an arbitrary set of AT baselines, might not exist. Different PRF selection approaches have been then formulated to achieve effective ambiguity rejection [12, 15]. However, the uncertainties in the knowledge of the real-time position (1 cm would be required in S-Band) and the limited accuracy on baseline control would make such strategies hard to implement with current technology. A swarmSAR formation demands therefore procedures to handle (on the ground) irregularly sampled pulses [8, 9, 16], as sketched in Fig. 3. Such problem has been investigated within the same project framework in [12], although the work addressed a slightly under-sampled scenario. The study conveyed that the AASR performance of swarmSAR images shall be regarded as stochastic, as far as the baselines cannot be precisely controlled. In the present work, the performance is analyzed for critically sampled nodes (with PRF set to the highest echo window, function of the incidence angle). The signal reconstruction is still based on the Best Linear Unbiased (BLU) interpolator [9, 12].

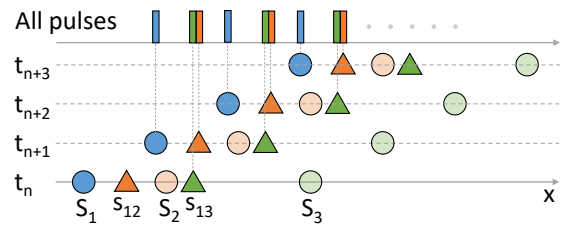


Fig. 3. Azimuth phase centers in a SIMO SAR system with 3 antennas, the first (S_1) transmitting and the other two ($S_{2,3}$), at physical locations marked with transparent circles, receiving. The figure addresses the transmission of 4 pulses along the aperture. The location of the equivalent phase centers for the bistatic acquisitions is represented with triangles.

The performance for a few representative SwarmSAR HR configurations, with 3 and 6 satellites, is reported in Table 2. The benefit of N transmitters in FDM for imaging is a straightforward enhancement by a factor N in the number of looks, or in the resolution. The benefits of the N receivers are rather identified in the augmented azimuth sampling. As mentioned above, however, this does not lead to an equivalent N times higher PRF, since the sampling is irregular. In the worst case the pulse might even be perfectly overlapping excluding any AASR benefit. Conversely, the N boost factor steadily applies to the NESZ. With reference to (1), it can be indeed roughly asserted that the NESZ in the final focused product is related to the number of satellites by

$$\text{NESZ}_{\text{swarm}} = \text{NESZ}_{\text{single}} / N \quad (2)$$

as the equivalent power increases by a factor N . Approximately 3 dB should be for instance gained by passing from 3 to 6 satellites, as Table 2 confirms. The improvements with respect to a single node, however, do not exactly match the N factor due to a difference in PRF and in resolution.

In order to render visually the improvements brought by the swarm we designed a SwarmSAR simulator based on 5m Stripmap Sentinel-1 images. A stack of 30 S1 images were multilooked in time, in order to preserve the resolution, and were adjusted to the NRCS levels of our system, i.e. the different incidence angles and frequency were accounted for. The experiment, illustrated in Fig. 4 on a small patch for a 30° incidence angle, clearly conveys the increase in quality (a Normalized Mean Squared Error (NMSE) on NRCS computed with respect to the original stack and displayed in dB) as a function of the number of satellites.

Finally, it can be further observed from Table 2 that the added value of a swarm also lays on the capability to illuminate larger swaths and wider access angle ranges than in single-node mode, by using lower PRFs while still easily satisfying the NESZ and DTAR requirements.

IV. SWARMSAR XT INTERFEROMETRY

The presence of a non-null XT baseline allows to resolve the scene scatterers in the third dimension, often referred to as cross-range. Cross-track interferometry processing includes both a straightforward (but still very relevant) multi-track InSAR option (or MIMO InSAR), aimed at measuring the surface elevation when a single scattering layer is assumed, or more complex tomographic options, aimed at reconstructing

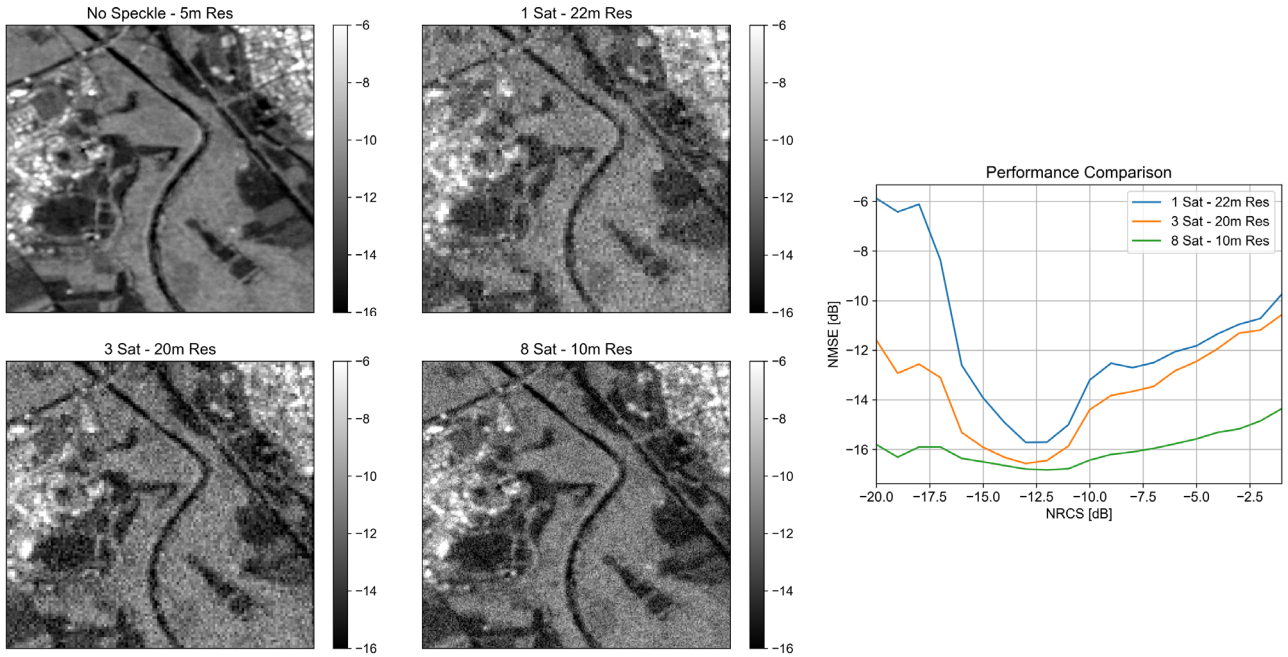


Fig. 4. Simulated HR imagery, for 30° incidence angle, from a NRCS dataset derived on a temporally averaged Sentinel-1 5m Stripmap stack. The stack was fed to the SwarmSAR simulation tools, where the IRF and the NESZ of the system (function of the number of satellites) has been applied. Notice that the resolution reported on the images refers to the product (pixel) resolution and not to the intrinsic one of the system. On the right the deviations from the S1 NRCS (in the top-left corner) is reported. Notice that the increase of the error for NRCS > -12 dB is due to a nuisance effect of the product resolution on point targets.

the vertical scattering profile through either non-parametric methods (simple 3D focusing) or model-based inversion (using coherence and phase models). As these methods exploit the coherent combination of the channels, one of the requirements of XTI interferometry is that the displacement or the changes of the scene (its scatterers) are small when compared to the wavelength during the acquisition time, which can be long for repeat pass interferometry. The fundamental benefit brought by a swarmSAR system consists in the opportunity to perform Single-Pass interferometry to avoid temporal decorrelation. The resolution capabilities in cross-range depend on many variables: the number of satellites, their perpendicular baselines, the incidence angle, the wavelength and the scatterers' characteristics.

MIMO InSAR

In the basic case of MIMO InSAR all the N^2 channels contribute to the estimation of a single parameter, i.e. the surface height. For such topography applications, the performance can be assessed by computing the Cramer Rao Lower Bound. Each channel observation can be modeled as

$$y_{rx} = x \cdot \exp\left(j \frac{2\pi}{\lambda} \frac{b_{rx,tx}}{R} v\right) + \omega_{tx} + \omega_{rx} \quad (3)$$

where $b_{rx,tx}$ is the baseline between the Tx and Rx antenna, v is the cross range of the target with respect to a reference target (whose phases have been subtracted from y), $x \sim \mathcal{CN}(0, \sigma_0)$ is the target speckle, and $\omega_{tx}, \omega_{rx} \sim \mathcal{CN}(0, \sigma_\omega)$ are the noises sources from the Tx and Rx. For each transmitter we have N observations and hence a vector $\mathbf{y} = [y_{rx1} \ \dots \ y_{rxN}]$ behaving as

$$\mathbf{y} \sim \mathcal{CN}(\mathbf{0}, \mathbf{R}), \quad \mathbf{R} = \sigma_0 \boldsymbol{\Phi} \boldsymbol{\Gamma} \boldsymbol{\Phi}^H + \boldsymbol{\Omega} \quad (4)$$

with $\boldsymbol{\Phi} = \left\{ e^{j \frac{2\pi}{\lambda} \frac{b_{rx,tx}}{R} v} \right\}_{ii}$ being a diagonal matrix with the phases of the target, $\boldsymbol{\Gamma}$ standing for the normalized coherence matrix and $\boldsymbol{\Omega} = 1/2 \text{ NESZ}(\mathbf{1} + \mathbf{I})$ recalling the noise covariance matrix, where it is assumed that NESZ is stronger than noise from DTAR, and hence $\sigma_\omega \cong \text{NESZ}/2$. Notice how, due to ω_{tx} in (3), in multi-static observations with a common transmitter the noises are not uncorrelated. By means of the Slepian-Bangs formula [11], the Fisher Information for a SwarmSAR can be formulated as

$$I(v) = L \cdot N \cdot \text{Tr} \left\{ \mathbf{R}^{-1} \frac{\partial \mathbf{R}}{\partial h} \mathbf{R}^{-1} \frac{\partial \mathbf{R}}{\partial h} \right\}. \quad (5)$$

The information is then readily converted into the standard deviation bound on height for an incidence angle θ through $\sigma_h = \sin \theta / \sqrt{I(v)}$. Expression (5) accounts for 3 factors. The first is the number of looks L on the ground used for the coherences. The second is the number of transmitting nodes N , conveying that the advantage of a MIMO over a single-transmitter system (SIMO) is a trivial enhancement of a factor N of the variance. The third term relates to the SIMO system. Such term is independent from the transmitter. Its behavior is mainly a function of the number of receiving nodes and of the baseline distribution. As shown in Fig. 5, the performance is characterized by a clear trend for baseline spreads lower than half of the critical baseline. Beyond such baseline spread the performance becomes increasingly variable for swarms with $N \leq 4$. The best performance is reached for quasi-uniform

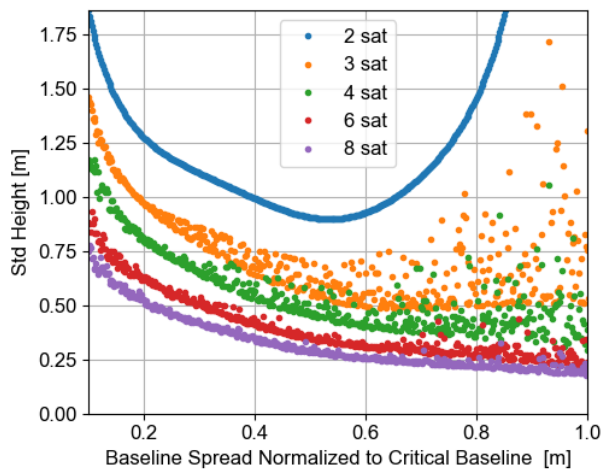


Fig. 5. MIMO InSAR performance of SwarmSAR on a 40m resolution product as a function of number of satellites and maximum perpendicular baseline of a pair for an incidence angle of 20° and an approximate critical baseline of 2.5 km. The baselines are randomly generated.

baseline distribution, whereas the performance drops correspond to skewed baseline distributions. Swarms with $N \geq 6$ are interferometrically more robust and can achieve 0.5 m vertical precision, see Fig. 5, on a 40 m ground resolution with baseline spreads < 500 m.

SAR Tomography

A tomographic SAR processing framework leverages on the assumption that multiple scatterers lay inside a single range-azimuth resolution cell, distributed in cross-range. A low finite number of scatterers is usually modelled for urban scenarios, whereas a continuous vertical scattering profile accounts for natural volumetric media, such as snow, ice and vegetation. In non-parametric processing, i.e. focusing in cross-range using beamforming techniques, the cross-range resolution is given by $2\lambda R/B$ where B is the perpendicular baseline spread, when the baselines are uniformly spaced. This means a 2 km baseline leads only to a resolution of 50 m in cross range and 17 m in height (at 20° incidence). Going beyond 2 km would make the observations unusable for the distributed scatterers. In a baseline operating mode, the S-Band SwarmSAR is hence better suited for model-based tomographic retrieval of point-target scatterers. Similarly to HR imaging, the added value of MIMO over SIMO is an increase of a factor N in the slant range resolution, as sketched in Fig. 6.

V. SWARMSAR CHALLENGES AND CONCLUDING REMARKS

The potential of a SwarmSAR in HR imaging and in XT interferometry has been outlined. Such potential comes, however, with a few challenges. A first challenge consists in determining the optimal width of the swarm orbital tube. Whereas the HR imaging would benefit from small XT baselines, and hence more common bandwidth, the XTI mode is rather demanding larger distances. The two processing schemes can however coexist well when XTI is used for MIMO InSAR.

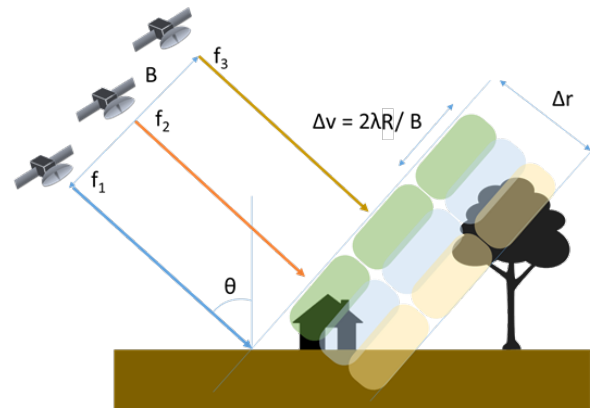


Fig. 6. MIMO SAR tomography principle illustrated. The slant range resolution Δr refers to the single-node resolution.

At system level, the SwarmSAR has to address more challenges regarding synchronization, downlink and attitude and orbit control aspects. At the current stage, the baseline concept envisions on-ground pre-processing and merging of all the channels. The phase synchronization shall hence be achieved on-ground through data-driven methods. Inter-satellite synchronization links are in principle not required. Pulse synchronization, i.e. adjusting the timing of the pulses to match the echo windows, shall be instead carried out on-board through GPS timing. Downlink capacity is also affected by this strategy as each node is expected to autonomously download the full raw data. With an overall duty cycle of 3% and 4-bits quantization, the data amount to a rough estimate of 60 Gbit per day per node. PreSum is not an option for HR imaging, since all the azimuth samples shall be used for signal reconstruction. With concern to the attitude and the orbits, the use of S-Band helps in relaxing the pointing and baseline requirements of a factor 3 with respect to more ‘conventional’ X-Band alternatives.

Further added value is expected in along-track interferometry and ground moving target identification (GMTI), although this aspect has not been covered in the paper. In light of all the raised considerations, we believe that future research on SwarmSAR should be aimed at extracting joint 4D information (space and velocity) from the data, rather than optimizing the formation configuration for each mode (HR vs XTI vs ATI) and address these latter in close compartments.

ACKNOWLEDGMENT

The work presented in this paper was carried out at Delft University of Technology within the frame of the project ‘Dutch network on small spaceborne radar instruments and applications (NL-RIA)’ funded by the Netherlands Organization for Scientific Research.

REFERENCES

- [1] C. Stringham et al., "The Capella X-band SAR Constellation for Rapid Imaging," IGARSS 2019 - 2019 IEEE International Geoscience and Remote Sensing Symposium, Yokohama, Japan, 2019, pp. 9248-9251.
- [2] "Satellite Mission ICEYE-X1," ICEYE, URL: <https://www.iceye.com/>
- [3] M. Zonno, M. Sanjuan-Ferrer, P. Lopez Dekker, R. Hanssen, F. Van Leijen, H. Skriver, R. Danielson, T. Nagler, L. Pedersen, O. Lang, A. Gabriele, M. Ludwig, A. Lecuyot, (2016). "Performance assessment

- for the high resolution and wide swath (HRWS) post-Sentinel-1 SAR system," ESA Living Planet Symposium proceedings, 2016.
- [4] P. Rosen, S. Hensley, S. Shaffer, W. Edelstein, Y. Kim, R. Kumar, T. Misra, R. Bhan, and R. Sagi, "The NASAISRO SAR (NISAR) mission dual-band radar instrument preliminary design," in 2017 IEEE IGARSS, July 2017, pp. 3832–3835.
- [5] M. Cohen, A. Larkins, P. L. Semedo and G. Burbidge, "NovaSAR-S low cost spaceborne SAR payload design, development and deployment of a new benchmark in spaceborne radar," 2017 IEEE Radar Conference (RadarConf), Seattle, WA, 2017, pp. 0903-0907.
- [6] Krieger, G. 2014. 'MIMO-SAR: Opportunities and Pitfalls'. IEEE Transactions on Geoscience and Remote Sensing 52 (5): 2628–45. <https://doi.org/10.1109/TGRS.2013.2263934>
- [7] G. Krieger et al., "MirrorSAR: A fractionated space radar for bistatic, multistatic and high-resolution wide-swath SAR imaging," 2017 IEEE International Geoscience and Remote Sensing Symposium (IGARSS), Fort Worth, TX, 2017, pp. 149-152.
- [8] G. Krieger, N. Gebert, and A. Moreira, "Unambiguous SAR signal reconstruction from nonuniform displaced phase center sampling," IEEE GRSL, vol. 1, no. 4, pp. 260–264, Oct. 2004.
- [9] M. Villano, G. Krieger, and A. Moreira, "Staggered SAR: High-Resolution Wide-Swath Imaging by Continuous PRI Variation," IEEE Transactions on Geoscience and Remote Sensing, vol. 52, no. 7, pp. 4462–4479, July 2014.
- [10] A. Freeman, "Design Principles for Smallsat SARs," 32nd Annual AIAA/USU Conference on Small Satellites, 2008.
- [11] S. Gao, Y. Rahmat-Samii, R. E. Hodges and X. Yang, "Advanced Antennas for Small Satellites," in Proceedings of the IEEE, vol. 106, no. 3, pp. 391-403, March 2018.
- [12] L. Iannini et al., "PRF Sampling Strategies for Swarmsar Systems," IGARSS 2019 - 2019 IEEE International Geoscience and Remote Sensing Symposium, Yokohama, Japan, 2019, pp. 8621-8624.
- [13] P. Stoica and R. Moses, Spectral Analysis of Signals. Englewood Cliffs, NJ: Prentice-Hall, 2005.
- [14] M. Younis, S. Huber, A. Patyuchenko, F. Bordonni and G. Krieger, "Performance Comparison of Reflector- and Planar-Antenna Based Digital Beam-Forming SAR," International Journal of Antennas and Propagation, 2009.
- [15] Graziano, M.D.; Renga, A.; Grasso, M.; Moccia, A. "PRF Selection in Formation-Flying SAR: Experimental Verification on Sentinel-1 Monostatic Repeat-Pass Data". Remote Sens. 2020, 12, 29.
- [16] D. Cerutti-Maori, I. Sikaneta, J. Klare and C. H. Gierull, "MIMO SAR Processing for Multichannel High-Resolution Wide-Swath Radars," in IEEE Transactions on Geoscience and Remote Sensing, vol. 52, no. 8, pp. 5034-5055, Aug. 2014